PLOS COMPUTATIONAL BIOLOGY

RESEARCH ARTICLE

Spatial models of pattern formation during phagocytosis

John Cody Herron[1,2], Shiqiong Hu[3], Bei Liu[3], Takashi Watanabe[3¤], Klaus M. Hahn[2,3], Timothy C. Elston[1,2,3*]

1 Curriculum in Bioinformatics and Computational Biology, University of North Carolina at Chapel Hill, Chapel Hill, North Carolina, United States of America, **2** Computational Medicine Program, University of North Carolina at Chapel Hill, Chapel Hill, North Carolina, United States of America, **3** Department of Pharmacology, School of Medicine, University of North Carolina at Chapel Hill, Chapel Hill, North Carolina, United States of America

¤ Current address: Cancer Center Division of Gene Regulation, Fujita Health University, Toyoake, Japan
* telston@med.unc.edu

Check for updates

OPEN ACCESS

Citation: Herron JC, Hu S, Liu B, Watanabe T, Hahn KM, Elston TC (2022) Spatial models of pattern formation during phagocytosis. PLoS Comput Biol 18(10): e1010092. https://doi.org/10.1371/journal.pcbi.1010092

Editor: Attila Csikász-Nagy, Pázmány Péter Catholic University: Pazmany Peter Katolikus Egyetem, HUNGARY

Received: April 11, 2022

Accepted: September 22, 2022

Published: October 3, 2022

Copyright: © 2022 Herron et al. This is an open access article distributed under the terms of the Creative Commons Attribution License, which permits unrestricted use, distribution, and reproduction in any medium, provided the original author and source are credited.

Data Availability Statement: The code and data used for this project is available on GitHub (https://github.com/elstonlab/PhagocytosisRosetteModel) and under the Zenodo archive: https://doi.org/10.5281/zenodo.6448430. Note that for counting podosomes, additional code is required from: https://github.com/elstonlab/PodosomeImageAnalysis.

Funding: This work was supported by grants from the National Institute of General Medical Sciences (NIGMS) to TCE (R35GM127145) and to KMH

Abstract

Phagocytosis, the biological process in which cells ingest large particles such as bacteria, is a key component of the innate immune response. Fcγ receptor (FcγR)-mediated phagocytosis is initiated when these receptors are activated after binding immunoglobulin G (IgG). Receptor activation initiates a signaling cascade that leads to the formation of the phagocytic cup and culminates with ingestion of the foreign particle. In the experimental system termed "frustrated phagocytosis", cells attempt to internalize micropatterned disks of IgG. Cells that engage in frustrated phagocytosis form "rosettes" of actin-enriched structures called podosomes around the IgG disk. The mechanism that generates the rosette pattern is unknown. We present data that supports the involvement of Cdc42, a member of the Rho family of GTPases, in pattern formation. Cdc42 acts downstream of receptor activation, upstream of actin polymerization, and is known to play a role in polarity establishment. Reaction-diffusion models for GTPase spatiotemporal dynamics exist. We demonstrate how the addition of negative feedback and minor changes to these models can generate the experimentally observed rosette pattern of podosomes. We show that this pattern formation can occur through two general mechanisms. In the first mechanism, an intermediate species forms a ring of high activity around the IgG disk, which then promotes rosette organization. The second mechanism does not require initial ring formation but relies on spatial gradients of intermediate chemical species that are selectively activated over the IgG patch. Finally, we analyze the models to suggest experiments to test their validity.

Author summary

Phagocytosis, the process by which cells ingest foreign bodies, plays an important role in innate immunity. Phagocytosis is initiated when antibodies coating the surface of a foreign body are recognized by immune cells, such as macrophages. To study early events in phagocytosis, we used "frustrated phagocytosis", an experimental system in which

(R35GM122596), as well as from the National Institute of Biomedical Imaging and Bioengineering to TCE (U01 EB018816). JCH received support from the NIGMS (5T32 GM067553). The funders had no role in study design, data collection and analysis, decision to publish, or preparation of the manuscript.

Competing interests: The authors have declared that no competing interests exist.

antibodies are micropatterned in disks on a cover slip. The cytoskeleton of cells attempting to phagocytose these disks organizes into "rosette" patterns around the disks. To investigate mechanisms that underlie rosette formation we turned to mathematical modeling based on reaction-diffusion equations. Building on existing models for polarity establishment, our analysis revealed two mechanisms for rosette formation. In the first scenario an initial ring of an intermediate signaling molecule forms around the disk, while in the second scenario rosette formation is driven by gradients of positive and negative pathway regulators that are activated over the disk. Finally, we analyze our models to suggest experiments for testing these mechanisms.

Introduction

All cells must be able to respond to changes in their environment, and often the proper response requires cells to adopt a new morphology. For example, cell shape changes occur during migration, division, and phagocytosis. Typically, these changes are initiated when receptors on the cell surface are activated by an external cue [1]. Receptor activation initiates a signaling cascade that results in spatiotemporal regulation of the actin cytoskeleton. The Rho family of GTPases are a class of signaling molecules that play key roles in this process [2–6]. These proteins act as molecular switches. They are in an inactive state when bound with GDP and become active when GDP is exchanged for GTP. Once active, Rho GTPases interact with effector molecules including those that regulate the actin cytoskeleton. Due to the nonlinear nature of the signaling pathways that regulate GTPase activity, understanding the molecular mechanisms that generate cell shape changes has proven challenging [1]. Therefore, many recent studies have turned to mathematical modeling to explore mechanisms capable of generating complex molecular structures [7–11].

Here we focus on Fcγ Receptor (FcγR)-mediated phagocytosis because of its biological importance in the innate immune response [12,13] and because phagocytosis provides an ideal system for studying how Rho GTPases organize the cytoskeleton into well-defined structures. Phagocytosis is initiated by the binding of the antibody immunoglobulin G (IgG) to FcγR. Upon FcγR clustering, receptor cross-linking leads to phosphorylation of activation motif domains, enabling downstream signaling [12–14]. To study the events that initiate phagocytosis under well-controlled conditions, IgG is micropatterned in small disks on a glass coverslip (Fig 1A). Because the antibody is attached to the coverslip it cannot be internalized, and the experimental system is therefore referred to as "frustrated" phagocytosis [15]. Following receptor activation, actin-enriched, adhesion-like structures termed podosomes [13,16,17] form in a circle around the IgG disk (Fig 1B and 1C). Podosomes classically have been considered rod or cone-like structures of dense actin [16,17]. However, we recently demonstrated an hourglass-like shape [18]. Podosomes recruit many additional molecules and are thought to coordinate interactions between the actin cytoskeleton and the extracellular matrix [16,17,19]. They also form the leading edge of the phagocytic cup [20,21], and have been referred to as "teeth" coordinating the "jaw" during phagocytosis [21]. The mechanisms responsible for podosome formation and patterning are not known. Therefore, we turned to mathematical modeling to establish sufficient conditions for pattern formation during frustrated phagocytosis.

Beginning with Turing's seminal paper [22] and continuing with developments by Gierer and Meinhardt [23] and Meinhardt [24], reaction-diffusion models have been used to investigate pattern formation in biological systems. These models rely on positive feedback to amplify

observing and analyzing single molecule conformational changes in living cells [42]. We made use of these techniques to visualize Cdc42 during frustrated phagocytosis (Figs 1D–1G and S1C). Cdc42 localized to the podosome rosette, with individual molecule tracks clustered near podosomes (Fig 1D–1G).

Taken together these results suggest podosome rosette organization involves localized Cdc42 activity but does not require active myosin-mediated force generation. The involvement of Cdc42 in rosette formation is also supported by other studies; Cdc42 levels are reduced when actin is reduced at the phagocytic site [43], and Cdc42 is recruited to the tips of pseudopodia early in phagocytosis [40,44]. Therefore, we decided to investigate if a mechanism involving Cdc42 might underlie formation of the podosome rosette.

Forming coexisting clusters of active GTPase

The core components of mathematical models for polarity establishment include an inactive form of a GTPase that is cytosolic and diffuses rapidly, an active form that is membrane bound and diffuses slowly, and positive feedback through autoactivation [7–11]. Additionally, these models often assume that mass is conserved and, therefore, do not include protein synthesis and degradation. In their simplest form, these models typically form a single polarity site [7–10,25]. Recent investigations have focused on establishing mechanisms that generate coexisting active GTPase clusters. Chiou *et al*. investigated a minimal model of a GTPase polarity circuit that assumed mass conservation and did not include any form of negative feedback [8]. They demonstrated how, in this model, local depletion increases the competition time between clusters so that coexistence is maintained over biologically relevant time scales. To generate stable coexisting sites requires the inclusion of protein synthesis and degradation [10,45,46], adding negative feedback to limit the growth of active cluster [10,46], or including an intermediate state of the Rho GTPase, so it cannot be immediately reactivated following deactivation [9]. We note that any of these mechanisms might underlie rosette pattern formation. However, the GAPs ARHGAP12, ARHGAP25, and SH3BP1 have been shown to play a role in phagocytosis [47]. Therefore, we focused on the Wave-Pinning GAP (WPGAP) model studied by Jacobs *et al*. in which negative feedback occurs through activation of a GAP [10].

The WPGAP model (Fig 2A, [10]) is described mathematically by the following set of reaction-diffusion equations:

$$\frac{\partial \mathrm{u}}{\partial \mathrm{t}} = bv + \gamma v\frac{\mathrm{u^n}}{\mathrm{K}^n + \mathrm{u^n}} - \sigma u - eGu + D_u\nabla^2 u,$$

$$\frac{\partial \mathrm{v}}{\partial \mathrm{t}} = -bv - \gamma v\frac{\mathrm{u^n}}{\mathrm{K}^n + \mathrm{u^n}} + \sigma u + eGu + D_v\nabla^2 v,$$

$$\frac{\partial \mathrm{G}}{\partial \mathrm{t}} = cug - dG + D_G\nabla^2 G,$$

$$\frac{\partial \mathrm{g}}{\partial \mathrm{t}} = -cug + dG + D_g\nabla^2 g,$$

where u is the concentration of active GTPase, v is the concentration of inactive GTPase, G is the concentration of active GAP, and g is the concentration of inactive GAP. The basal GTPase activation rate is b, the maximum self-positive feedback rate is γ, K is the concentration of active GTPase when the feedback is at the half-maximal response, the basal GTPase inactivation rate is σ, the GAP-mediated negative feedback rate is e, the GAP activation is c, and the

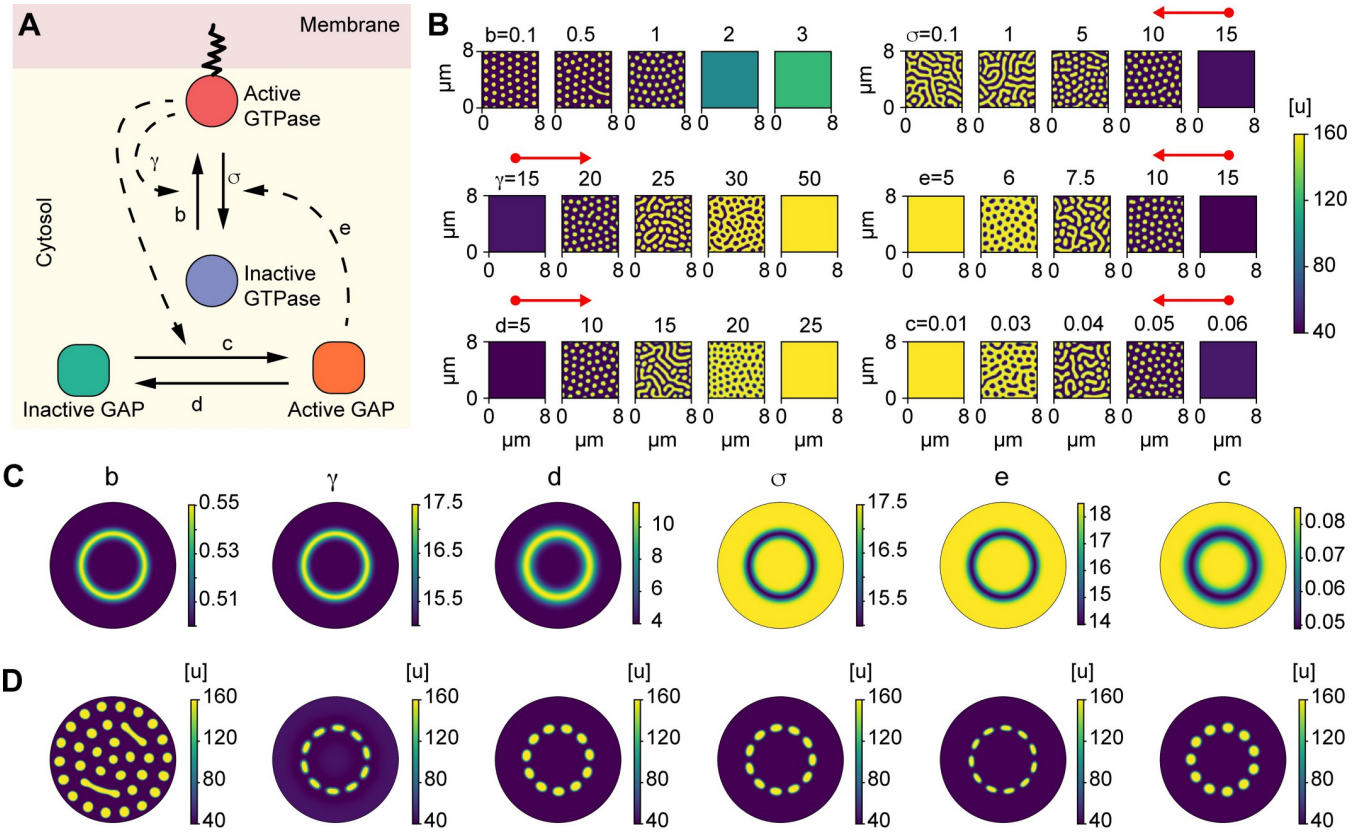

Fig 2. The WPGAP model generates rosettes of GTPase activity if a ring of an intermediate species is assumed. A) Schematic of the Wave-Pinning GTPase Activating Protein (WPGAP) model. **B)** WPGAP simulation results for individual parameter sweeps (Table 1). Red arrows show most parameters can transition from a low intensity homogenous regime (circle cap) to a spot patterning regime (arrow cap). **C)** Spatial profile of parameters modulated by species M. M either activates (first 3 panels) or inhibits (last 3 panels) parameters. **D**) Active GTPase concentrations using the parameter profiles shown in **C** (above each panel, respectively). Consistent with parameter sweeps shown in **B**, each parameter is capable of being modulated to form a rosette pattern except for the basal activation rate *b*.

https://doi.org/10.1371/journal.pcbi.1010092.g002

GAP inactivation rate is *d*. The total mass of both species is conserved:

$$T = \int (u + v)\, dV,$$

$$T_g = \int (G + g)\, dV,$$

where the integrals are over the volume of the system. A requirement for polarization is that the membrane-bound active form of GTPase diffuses slowly in comparison to the cytosolic inactive form:

$$D_v >> D_u.$$

Both the active and inactive forms of the GAP are treated as cytosolic species that diffuse rapidly compared to the membrane-bound active GTPase.

It is tempting for simplicity and computational efficiency to perform initial investigations on a 1D ring to find regions of parameter space that support coexisting spots. However, the existence of coexisting clusters on a 1D ring does not guarantee a localized ring of clusters will form when the system is extended to 2D. One important difference between 1D and 2D is that

in 2D spots have curvature, which can contribute to their stability [8]. Furthermore, our system requires low activity without patterning away from the spots, which could not be captured in 1D. Therefore, we performed WPGAP simulations in 2D.

For the WPGAP model, Jacobs *et al.* [10] explored how changes in the total amount of GTPase (T) impacted bistability and the types of patterns that formed. They found the system could form spots (localized regions of high GTPase activity), mazes, and negative spots (localized regions of low GTPase activity). In this study, we are interested in coexisting spots, and thus, guided by the work of Jacobs *et al.* [10], we began with parameter values that placed the system in this regime. From single particle tracking during frustrated phagocytosis (Fig 1D–1G), we estimated the diffusivity for the membrane-bound form of Cdc42 as ~0.04 $\mu m^2\ s^{-1}$ (S1C Fig). Using this information, we fixed $D_u = 0.04\ \mu m^2\ s^{-1}$ and we let $D_v = D_g = D_G = 100\ D_u$. Radii of podosomes have been observed to be anywhere from ~0.15–0.6 microns [17,18,48,49]. Therefore, we tuned the rate constants (Table 1) so that the model produced spots with radius 0.31 ± 0.02 μm. Because most of the rate constants in the model have not been measured experimentally, our choices for the initial parameter values are somewhat arbitrary. However, these rate constants result in coexisting spots of appropriate size when using the estimated membrane-bound diffusion coefficient for Cdc42.

To explore how GTPase cluster size depends on the relative time scales of diffusion and chemical kinetics, we fixed the rate constants and varied the diffusion coefficient of the active GTPase D_u, keeping the other diffusion coefficients 100-fold greater than D_u (S2A Fig). Note that mathematically this is equivalent to fixing the diffusion coefficients and varying the time scale for the chemical kinetics, because solutions to the model equations only depend on the ratio of these two time scales. We found that increasing the diffusivity increased the spot size (S2A and S2B Fig), but did not impact the patterns formed by the system (quantified by spot eccentricity, S2C Fig).

We set the average Cdc42 concentration to 808 molecules per μm^2 (Table 1). The number of Cdc42 molecules per podosome is not known. However, particle-based simulations of Cdc42 polarity in yeast typically predict around 3000 molecules in a polarity site of roughly 1 μm radius, resulting in a surface concentration of ~950 molecules per μm^2 [50]. Using a GTPase spot radius of 0.31 μm, the area of a podosome is approximately 0.30 μm^2, and there are approximately 240 Cdc42 molecules per podosome. This produces a surface concentration

Table 1. Baseline parameter values.

Parameter	Description	Value
b	GTPase activation	$1\ s^{-1}$
γ	GTPase maximal self-positive feedback rate	$20\ s^{-1}$
K	Half-maximal response GTPase concentration	200 molecules per μm^2
n	Hill coefficient	2
σ	GTPase inactivation	$10\ s^{-1}$
c	GAP activation	$0.05\ \mu m^2\ s^{-1}$
d	GAP inactivation	$10\ s^{-1}$
e	GAP dependent GTPase inactivation	$10\ \mu m^2\ s^{-1}$
D_u	Active GTPase diffusion	$0.04\ \mu m^2 s^{-1}$
D_v	Inactive GTPase diffusion	$4\ \mu m^2 s^{-1}$
D_G	Active GAP diffusion	$4\ \mu m^2 s^{-1}$
D_g	Inactive GAP diffusion	$4\ \mu m^2 s^{-1}$
T	Total GTPase Concentration	808 molecules per μm^2
T_g	Total GAP Concentration	10 molecules per μm^2

https://doi.org/10.1371/journal.pcbi.1010092.t001

of ~900 molecules per μm^2 at active spots, which is consistent with particle-based models for the polarity site in yeast.

Next, we explored how varying individual parameters changed pattern formation. When sweeping the GTPase activation rate *b*, lower values resulted in spots, but higher values resulted in a spatially homogenous steady state with an intermediate level of GTPase activity (Fig 2B). This suggested that a finite basal GTPase activation rate *b* was not required or had to be quite small to facilitate patterning. Interestingly, each of the other parameter sweeps resulted in changes in the observed patterning types, including spots, mazes, and holes (Fig 2B). For the GTPase inactivation rate σ, a high value resulted in a single low concentration throughout the domain, and decreasing this value led to spots, then mazes. However, minimizing this value did not cause the entire domain to be at a single, high steady state, due to negative feedback from GAPs. In contrast, the self-positive feedback rate γ, the GAP inactivation rate *c*, the GAP activation rate *d*, and the GAP-mediated negative feedback rate *e* were capable of all patterning types, from a single low state to spots, mazes, holes, and a single high state (Fig 2B). Overall, these observations suggested that it would be possible to spatially modulate these parameters to go from the low, homogenous state to the spot forming state.

A two-step model for rosette formation

We next sought to determine if the WPGAP model could be modified to enable rosette formation. One possible explanation for how a rosette could form is if two distinct steps occur: 1) an initial ring of high or low concentration of some species (M) forms and 2) this species modulates a key parameter in the pattern forming, WPGAP model. To test this model, we assumed a preexisting ring in the concertation profile of M. We note that rings of high GTPase activity have been observed and modeled in other contexts, such as in wound healing, in which a chemical gradient and modulation of a bistable GTPase resulted in distinct rings of activity [32,33].

For our initial investigations, we assumed that a modulator M affected a rate in the WPGAP model through the functional form:

$$\omega_{\pm}(r) = \omega_1 \pm \omega_2 M(r),$$

where ω_1 is the basal rate, ω_2 models the effect of M on $\omega_{\pm}$ and *r* measures the radial distance from the center of an IgG disk. In our simulations, we consider a single IgG disk and use polar coordinates with the origin located at the center of the disk. The computational domain consists of a disk of radius of R with reflective boundaries at r = 0 to r = R (see Methods). Unless otherwise noted R = 4 μm. M(r) was modeled as a Gaussian-shaped function centered at r = 2 μm with variable variance. This form of $\omega_{\pm}$ allowed us to tune model parameters so that spot formation was only promoted within the ring.

For parameters that increase GTPase activity (GTPase activation *b*, GAP inactivation *d*, and the maximum self-positive feedback rate γ), the WPGAP model was coupled to a ring of high M concentration ω_+ (Fig 2C and 2D, three leftmost columns). For parameters that decrease GTPase activity (GAP activation *c*, GTPase inactivation σ, and GAP-mediated GTPase inactivation *e*), the WPGAP model was coupled to an inverted ring of M, ω_- (Fig 2C and 2D, three rightmost columns). For each model parameter, ω_1 and ω_2 were varied to determine if the system could generate rosette organization. As an initial guess, the parameter values were chosen based on the results from the parameter sweeps (Fig 2B).

As expected from the parameter sweep results, modulating the basal GTPase activation rate *b* did not appear sufficient to form a rosette pattern, because this produced spot formation throughout the entire domain. However, modulating the other rate constants, such as the positive feedback rate γ, all resulted in a rosette forming (Fig 2C and 2D). Interestingly, when we

modulated the rates for GTPase inactivation σ and the GAP-mediated negative feedback e, we found that the rates required to form rosettes were higher than expected (Fig 2C and 2D). For example, to form a rosette, the rate required for the GTPase inactivation σ within the ring was ~15 s^{-1}, which resulted in no patterning when used as the global rate in the isolated WPGAP model (Fig 2B–2D).

Gradient establishment by a simple reaction-diffusion model

The analysis presented above demonstrated that the rosette pattern can form following the establishment of a ring of activity. Therefore, we next wanted to determine if rosette formation could occur in the absence of such an initial ring. Our first goal was to establish the concentration profile of a signaling molecule that is activated by IgG-bound receptors over the disk and deactivated throughout the domain. This profile was later used to model the spatially-dependent rate constants in the WPGAP model. Let X represent the active form of this molecule. To model the spatiotemporal dynamics of X, we used the following equation:

$$\frac{\partial \mathrm{X}}{\partial \mathrm{t}} = k_x(r) - \delta_x X + \frac{D_x}{r}\frac{\partial}{\partial r}\left(r\frac{\partial}{\partial r}\right)X$$

where $k_x(r)$ is the spatially-dependent activation rate, δ_x is the deactivation rate and D_x is the diffusion coefficient for X (Fig 3A). Note that if k_x is independent of r, then at steady state X(r) = k_x/δ_x. To model the IgG disk, we treat $k_x(r)$ as a step-function:

$$k_x(r) = \begin{cases} k_{disk} \text{ if } r < \mu_F, \\ k_{basal} \text{ if } r \geq \mu_F, \end{cases}$$

where k_{disk} is the IgG-induced activation rate, k_{basal} is the basal activation rate, and μ_F is the radius of the disk. For fixed values of k_{disk}, k_{basal}, and δ_x, this system was simulated for varying diffusion coefficients D_x (Fig 3B). The range of diffusion coefficients was chosen to approximate the orders of magnitude observed in cellular diffusion rates [51,52], from a slow membrane-bound rate (10^{-3} $\mu m^2 s^{-1}$) to a fast cytosolic rate (10.0 $\mu m^2 s^{-1}$). For a domain with a radius R = 4 μm, changing the diffusivity of X resulted in changes in both the gradient steepness and the difference between the maximum and minimum values of X (Fig 3C). For small values of D_x, the distribution of X was switch-like, and X approached the expected steady state, $k_x(r)/\delta_x$. However, for larger values of D_x, the gradient in X was shallower, and deviated significantly from $k_x(r)/\delta_x$ with a lower total amplitude (Fig 3B and 3C). We wondered if there was a functional form that approximated the solution to this equation, and found that our simulation results could be well approximated using a logistic function with the form:

$$f(r) = \beta + \frac{\alpha}{1 + \exp\left(k_m(r - r_0)\right)},$$

where β and $\alpha+\beta$ are the minimum and maximum values of f(r), respectively, k_m is the logistic decay rate, and $f(r_0) = \beta+\alpha/2$ (Fig 3D). Therefore, for simplicity and computational speed we used f(r) when performing parameter searches for the WGAP model. However, after performing parameter searches, we then verified that directly simulating the diffusing species rather than using f(r) also generated rosette formation (see S1 Note).

Rosette formation through gradients

To determine if rosette formation is possible in the WPGAP model without the formation of an initial ring around the IgG disk, we treated the positive feedback rate γ and the GAP

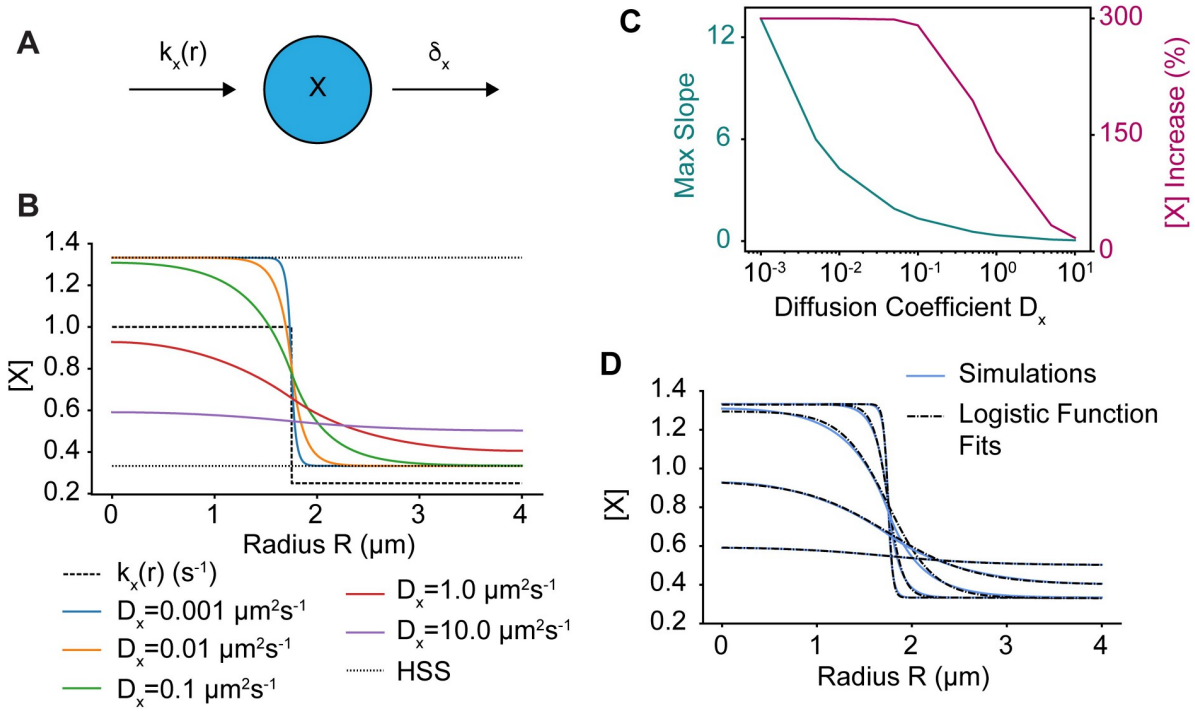

Fig 3. A simple reaction-diffusion model for gradients of activity. A) Schematic of the simple reaction-diffusion model in which a species X is activated by a rate $k_x(r)$, which depends on the local IgG concentration, and is deactivated at a constant rate δ_x. **B**) Simulations of the model for various diffusion rates D_x. The spatial profile of $k_x(r)$ is shown as the dashed line and $\delta_x = 0.75\ s^{-1}$. The homogenous steady states values of X when k = $k_x(0)$ and k = $k_x(r_{max})$ are shown as well (dotted lines). **C)** Maximum slope of X(r) and percent increase of X(0) over X (r_{max}) as a function of D_x. **D)** Blue curves are same as in **B** and dashed lines are best fits of these curves to the logistic function (see Methods for curve fitting details).

https://doi.org/10.1371/journal.pcbi.1010092.g003

activation rate c as spatially-dependent with profiles given by f(r):

$$\gamma(r) = \gamma_\beta + \frac{\gamma_\alpha}{1 + \exp(\gamma_{km}(r - r_0))},$$

$$c(r) = c_\beta + \frac{c_\alpha}{1 + \exp(c_{km}(r - r_0))}.$$

Note that these functions asymptotically approach their maximum values of $\gamma_{max} = \gamma_\alpha + \gamma_\beta$ or $c_{max} = c_\alpha + c_\beta$ as r decreases.

Unlike the two-step model, it was difficult to empirically determine parameter values that form a rosette. Thus, we used a two-step approach to search parameter space. We first used an evolutionary algorithm (EA) [53] to perform a global search and subsequently performed a more local sampling of parameter space using a Delayed Rejection Adaptive Metropolis Markov chain Monte Carlo (DRAM-MCMC, see Methods) [54,55].

To implement the two-step approach requires a score function that provides a quantitative measure for how close a simulated result is to the desired rosette pattern. For the desired pattern, a GTPase rosette formed by the two-step model was used (Fig 2D). From this, we measured the radial average and radial standard deviation for the active GTPase u (Fig 4A–4C). For new simulations, we measured the radial average of u (Fig 4A and 4C). We then divided the system into octants and measured the radial standard deviation within each octant (Fig 4B and 4C). The difference between the means of the desired output and simulation result and

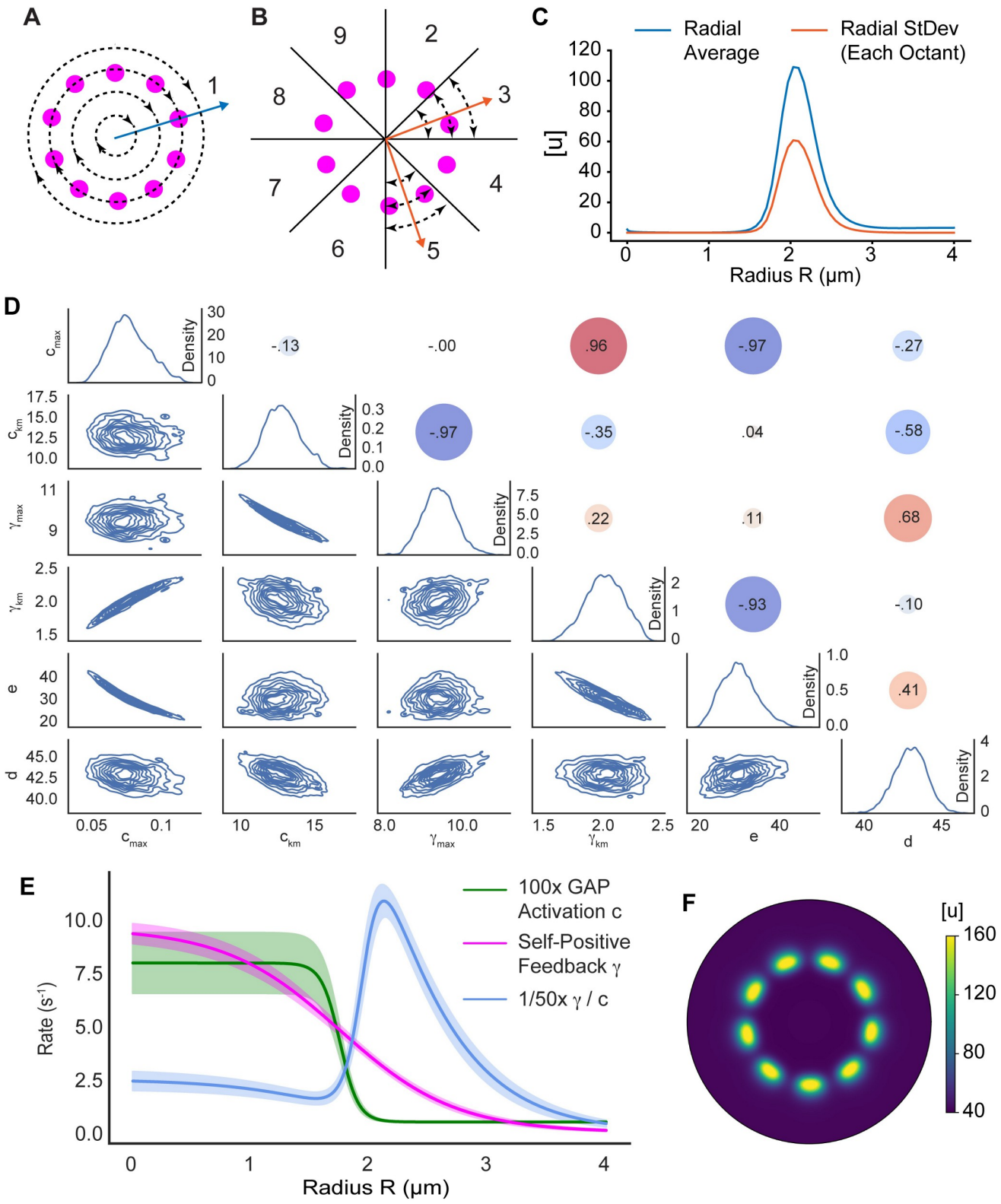

Fig 4. Model parameterization reveals mechanism enabling rosette formation. A) Schematic illustrating the radial averaging of GTPase activity used in the score function. **B)** Schematic illustrating the radial standard deviation of GTPase activity per octant used in the score function. This results in eight individual quantifications used in the score function. **C)** Radial profiles of the average and standard deviation of GTPase activity. These profiles were used in the score function and compared to the results from numerical simulations. **D)** Parameter distributions after performing DRAM-MCMC sampling.

Individual parameter distributions are shown on the diagonal. Lower triangular plots show kernel density estimates for parameter pairs. Circles in the upper triangle represent the Spearman correlation coefficient between parameters. **E)** Radial profiles for the non-constant parameters from the parameter estimation. The positive to negative feedback ratio is also shown. For visualization purposes, the GAP activation rate and ratio are scaled to be similar orders of magnitude. The solid lines are the results for the mean parameter values from **D** (on the diagonal, Table 2) and the shaded regions indicate one standard deviation. **F)** Active GTPase concentration using the representative parameter set (Table 2). Simulation domain has a max radius of 4.0 μm.

https://doi.org/10.1371/journal.pcbi.1010092.g004

the differences between the standard deviation of the desired output and standard deviations in each octant were calculated. These nine measurements (Fig 4A–4C) were then averaged to produce a single score. This score function was accurate, but flexible enough to allow for various numbers of spots and spot locations.

Simulations were initialized with a small amount of random noise and seeded with an initial concentration of active GTPase in the shape of a rosette (see Methods). We seeded simulations with a rosette to decrease the time for pattern formation, because parameter estimation requires a significant number of simulations. Also, from observations of initial parameterization attempts, the GTPase activation rate b, the GTPase inactivation rate σ, the minimum self-positive feedback rate γ_α, and the minimum GAP activation rate c_α were typically quite small and were thus fixed at 2e-3, 0.4, 5e-3, and 5e-3 s^{-1}, respectively. For 99 individual EA runs (100 individuals, 100 generations), most runs were able to discover parameters capable of rosette organization (top 80 appeared successful, S3A and S3B Fig). The best parameter set found by the EAs was then used to initialize DRAM-MCMC simulations. DRAM-MCMCs were simulated until they appeared to converge, with all but the final 5,000 iterations removed as a "burn-in" period (S3C Fig, see Methods).

The parameter distributions generated by MCMC sampling appeared Gaussian (Fig 4D, on the diagonal). We took the mean values of the individual parameter distributions as our representative parameter set (Figs 4D–4F and S3D and Table 2). To check how well the MCMC performed, we also simulated the worst scoring parameter set, and these parameters also resulted in rosette organization (S3D and S3E Fig and S1 Table). Our simulations predicted that GTPase rosettes mostly form by 20 s and appear stable by 40 s (S4 Fig). We also verified that simulating the diffusing species (see the section Gradient Establishment by a Simple Reaction-Diffusion Model) rather than using the logistic function approximation f(r) would generate rosette formation (see S1 Note, S5 Fig).

Inspection of the spatially-dependent rates revealed how the system was capable of rosette patterning (Fig 4E). When the ratio between the positive to negative feedback ($\gamma(r)/c(r)$) is plotted as a function of r using the identified parameter sets, in all cases the ratio is maximized just beyond r = 2 μm, near where the spots formed (Fig 4E and 4F). Relative to the self-positive feedback rate $\gamma(r)$ (Fig 4G, magenta), the GAP activation rate $c(r)$ (Fig 4E, green) is high over the disk and away from the disk. However, c transitions more rapidly than γ between its elevated level over the disk and its basal level away from the disk (Fig 4E). Thus, while the negative feedback is relatively high over the disk and away from it, there is a zone near the edge of the disk where the negative feedback is low relative to the positive feedback. It is in this region that rosette formation occurs.

To gain further insight into the model's behavior we looked for pairwise correlations between model parameters. Several parameters demonstrated strong correlations (Fig 4D). There was a strong anti-correlation between c_{max}, the maximum GAP activation rate, and e, the rate constant for GAP-mediated GTPase inactivation. This likely indicates a sensitivity of the model to the total amount of GAP activity. The other correlations were not as intuitively apparent, so to further explore parameter-dependent model behavior, we performed individual parameter sweeps using the representative parameter set (Table 2 and Fig 5A–5F). Parameters typically moved from no patterning to rosette organization to ring formation (c_{km}, γ_{max},

Table 2. Mean parameter set after MCMC parameterization.

Parameter	Description	Value (± StDev)	Fixed or Sampled
b	GTPase activation	0.002 s^{-1}	Fixed
γ_{max}	GTPase self-positive feedback rate, maximum spatial value	9.6 ± 0.5 s^{-1}	Sampled
γ_{km}	GTPase self-positive feedback rate, decay rate	2.04 ± 0.16	Sampled
γ_{α}	GTPase self-positive feedback rate, minimum spatial value	0.005 s^{-1}	Fixed
K	Half-maximal response GTPase concentration	200 molecules per μm^2	Fixed
n	Hill coefficient	2	Fixed
σ	GTPase inactivation	0.4 s^{-1}	Fixed
c_{max}	GAP activation, maximum spatial value	0.08 ± 0.01 $\mu m^2 s^{-1}$	Sampled
c_{km}	GAP activation, decay rate	13.0 ± 1.2	Sampled
c_{α}	GAP activation, minimum spatial value	0.005 $\mu m^2 s^{-1}$	Fixed
d	GAP inactivation	43.0 ± 1.1 s^{-1}	Sampled
e	GAP dependent GTPase inactivation	31.3 ± 4.4 $\mu m^2 s^{-1}$	Sampled
D_u	Active GTPase diffusion	0.04 $\mu m^2 s^{-1}$	Fixed
D_v	Inactive GTPase diffusion	4 $\mu m^2 s^{-1}$	Fixed
D_G	Active GAP diffusion	4 $\mu m^2 s^{-1}$	Fixed
D_g	Inactive GAP diffusion	4 $\mu m^2 s^{-1}$	Fixed
T	Amount of GTPase	808 molecules per μm^2	Fixed
T_g	Amount of GAP	10 molecules per μm^2	Fixed

https://doi.org/10.1371/journal.pcbi.1010092.t002

and d, Fig 5B, 5C and 5E), or vice versa (c_{max}, γ_{km}, and e, Fig 5A, 5D and 5F). Thus, the anti-correlations between c_{km} and γ_{max} as well as γ_{km} and e likely result from a balancing of the effects produced by varying the individual parameters. However, the reason for the positive correlation between c_{max} and γ_{km} is not readily apparent but may result from the logistic function having a lower maximum value for shallower gradients (i.e., low decay rates, Fig 3). Also, note that this model can generate rings of activity (Fig 5A–5F), as is required for the two-step model discussed above.

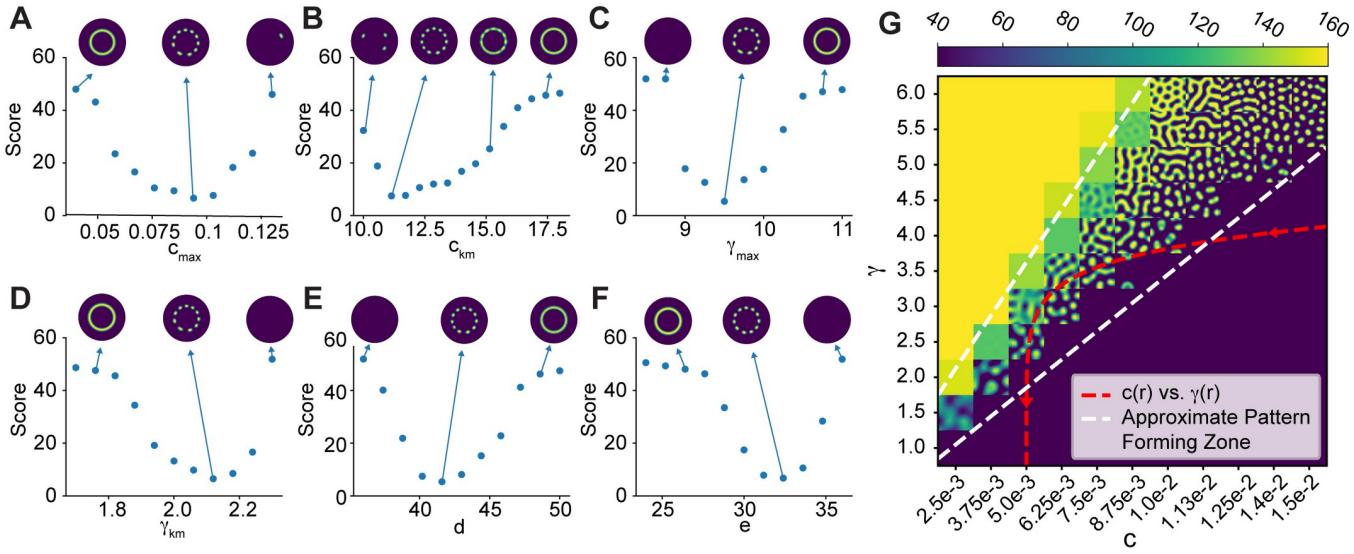

Fig 5. Effects of individual parameters on patterning. A-F) Plots of the score function versus model parameters (Table 2). Representative simulation results shown to illustrate the impact of varying parameter values on rosette formation. **G)** Two parameter sweep varying c and γ. Each grid cell shows the active GTPase concentration for an individual simulation when c and γ are fixed. The red dashed line is a plot of $c(r)$ versus $\gamma(r)$ from Fig 4E and Table 2.

https://doi.org/10.1371/journal.pcbi.1010092.g005

Fluor 568 phalloidin (dilution 1:500, ThermoFisher Scientific A12380) diluted in 2% BSA in PBS at room temperature for 20 min followed by one wash with 1xPBS/0.05% Tween for 10 min, and two washes with 1x PBS for 15 min.

Imaging of podosome structures during frustrated phagocytosis

Total internal reflection fluorescence structured illumination microscopy (TIRF-SIM) was used to image podosomes in F-tractin-tdTomato transfected live RAW 264.7 macrophages. Fluorescence emission was recorded using an sCMOS camera (Hamamatsu, Orca Flash 4.0 v2 sCMOS). Lasers with wavelengths 560 and 647 nm and an Olympus UApo N 100x oil NA 1.49 objective were used, and fluorescence emission was recorded using an sCMOS camera (Hamamatsu, Orca Flash 4.0 v2 sCMOS). A Nikon SIM microscope was used to image podosomes in fixed RAW 264.7 macrophages after Y-27632 inhibition, using 488 and 561 nm lasers. A 100x oil immersion objective (1.49 NA, Nikon CFI Apochromat TIRF 100x) and EMCCD camera (Andor DU-897) were used. To image podosomes in bone marrow-derived macrophages, a Zeiss confocal microscope LSM880 built around AxioObserver 7 with a 63x 1.4 NA oil objective (Zeiss) was used.

Single particle tracking

Single particle tracking was performed using a home-built total internal reflection microscope based on an Olympus IX81. The microscope was equipped with four solid state lasers (Coherent OBIS 405 nm, 488 nm, 561 nm, and 647 nm), a 100X TIRF objective (Olympus, UPLAPO100XOHR) and an sCMOS camera (Photometrics Prime 95B) for fluorescence collection. Raw cells were co-transfected with mScarlet-F-tractin (Excitation, 561 nm; Emission, Semrock, FF01-600/52) and Cdc42-HaloTag [68]. Note that the HaloTag was attached to the N terminus of Cdc42 to ensure that membrane interactions were not impaired. Cells were incubated with 100 pM dye JF646-Halo (Emission, Semrock, FF01-698/70) for 30 minutes and washed with culture medium three times before imaging. Super-resolved F-tractin images were acquired at 100 Hz for 5 seconds and subjected to Super-Resolution Radial Fluctuations analysis [69]. For single particle tracking of Cdc42, we streamed for 40 seconds at 50 Hz (2000 frames).

Single molecule diffusion analysis was done as before [42]. Briefly, individual molecules were identified by a wavelet decomposition based approach [70] and precise centroids were obtained by fitting with a 2D Gaussian function. Single molecule trajectories were built through a well-established linking algorithm [71] and the mean-square-displacement was then calculated [72,73] to color encode the tracks.

Numerical simulations

Ordinary differential equation (ODE) simulations were performed by using the Python package odeint from Scipy [74]. Reaction-diffusion equations were solved using the spectral differential equation solver Python package Dedalus [75]. For simulations using Cartesian coordinates, the system was spatially discretized using a Fourier basis in x and a Chebyshev basis in y with the recommended dealiasing factor of 1.5, as done before [10]. The system had periodic boundary conditions in x and Neumann (reflective) boundary conditions in y. Similarly, for simulations using polar coordinates, the system was spatially discretized using a Fourier basis in ϕ, and a Chebyshev basis in r (dealiasing factor of 1.5) with periodic boundary conditions in ϕ, and Neumann (no flux) boundary conditions in r. The typical grid size used for simulations was 256 x 128 (ϕ, r respectively) which was informed by mesh grid refinement (i.e., larger grid sizes resulted in the same outcome). However, a grid size of 64 x 64 was used for parameterization steps to decrease simulation time. Simulations were typically performed

using a time step dt = 0.01 s or 0.025 s. Reaction steps were solved using 4th order Runge-Kutta, although 2nd order Runge-Kutta was used for parameterization steps.

Homogeneous steady states were determined by running the ODE system (without diffusion) for t = 1000 s using odeint. For initial conditions of the reaction-diffusion equations, each species was set to its steady state value throughout the domain and subsequently noise was added by converting a small fraction of inactive species to the active form. The fraction of concentration converted was determined by each simulation but was typically generated by uniform sampling between 0 and $0.2v_{ss}$ (where v_{ss} is the steady state concentration for the inactive species). For seeded simulations, the same random noise (but between 0 and $0.1v_{ss}$) was converted and additionally the normalized seed (i.e., a rosette) was scaled by $0.1v_{ss}$ and converted to active GTPase. For simulations with non-constant coefficients, the initial steady states were determined by using the basal values for the spatially-dependent rates.

To fit the logistic equation to the simple reaction-diffusion profiles, we used the Python package minimize (using method = "SLSQP") from Scipy [74].

Parametrization

Evolutionary algorithm (EA) simulations were performed using the Python package DEAP (v1.3.1) [53]. For EA hyperparameters we used a mutation rate of 0.3 and a crossover rate of 0.5. Markov chain Monte Carlo (MCMC) simulations were performed using the Python package Pymcmcstat (v1.9.1) [55]. For MCMC sampling, we used the Delayed Rejection Adaptive Metropolis (DRAM) algorithm [54,55]. MCMC hyperparameters were set to S20 = 0.015 and N0 = 0.015, which resulted in chain acceptance rates between 29–40%. Chains were run for between 10,000–12,500 steps. All but the last 5,000 steps for individual MCMC chains were discarded as a "burn-in" period. MCMC chains appeared to pass all convergence tests, including within chain variance (Geweke statistic $p >> 0.05$, [76]) and between chain variance (Gelman-Rubin diagnostic < 1.1, [77]).

Note that for the coupled model, where the simple reaction diffusion model was simulated in place of the logistic function, we used the same MCMC pipeline for sampling to discover a working coupled model. For proof of concept, we simply ran this pipeline for 1,000 steps and took the best scoring parameter set.

Spot size determination

Simulations were performed as described above using cartesian coordinates (t_{final} = 40 s). Each system was interpolated to a uniform grid with the same grid size (128 x 128). A mask was generated by thresholding at the mean of the maximum and minimum concentrations within the system. Using this mask, features were quantified using the Python package scikit-image [78]. The effective radius was defined as the average between the major and minor axis lengths. After an initial pass at fitting Radius$_{eff}$ based on log(D_u), simulations were rerun using different grid sizes to ensure the number of spots counted for each simulation were similar (N~100).

Counting podosomes per site

For experimental results, the number of podosomes per site were calculated using a pipeline we developed previously [18] (https://github.com/elstonlab/PodosomeImageAnalysis). In essence, this pipeline uses persistent homology, a type of topological data analysis, to identify significantly persistent features (connected components, holes) within images followed by post-processing.

S1 Note

In the main manuscript, the profiles of the spatially dependent rates $\chi(r)$ and $c(r)$ were prescribed using the logistic function $f(r)$. Therefore, we wanted to confirm that when we use the solution to the equation for a diffusing species X that is activated over the disk to generate spatial profiles for the chemical species that modulate $\chi(r)$ and $c(r)$, the system still generates a rosette pattern. As noted in the main text the equation for X is:

$$\frac{\partial X}{\partial t} = k_x(r) - \delta_x X + \frac{D_x}{r}\frac{\partial}{\partial r}\left(r\frac{\partial}{\partial r}\right)X$$

$$k_x(r) = \begin{cases} k_{disk} \; if \; r < \mu_F, \\ k_{basal} \; if \; r \geq \mu_F, \end{cases}$$

where $k_x(r)$ is the spatially dependent activation rate, δ_x is the deactivation rate and D_x is the diffusion coefficient for X, k_{disk} is the IgG-induced activation rate, k_{basal} is the basal activation rate, and μ_F is the radius of the disk.

Surprisingly, however, fitting solutions for X to $\chi(r)$ and $c(r)$ from the main text (logistic function approximation) and using these solutions in the WPGAP model did not lead to proper rosette formation. This discrepancy likely arises from slight differences between the logistic function and solutions to the reaction-diffusion equation (Fig 3D). Therefore, we used the parameter values found from

fitting $\gamma(r)$ and $c(r)$ to initialize another DRAM-MCMC run that included equations for species that modulate $\gamma(r)$ and $c(r)$. Because our goal was to simply demonstrate proof of principle, we only performed 22 short (1000 iterations) DRAM-MCMC runs, and we took the single best scoring parameter set. However, this was sufficient to demonstrate that a model that explicitly considered species that modulate $\gamma(r)$ and $c(r)$ was able to generate a GTPase rosette (S5 Fig, S1 Note Table A, below). In S5C,D Fig, we plot the distributions of the species modulating the rates for the GAP activation rate, c, and the self-positive feedback rate, γ, respectively. Interestingly, if these profiles are used to modulate the intermediate species M in the two-step model, the system creates a ring of active M (as in S5E Fig). Thus, the same mechanism where the positive feedback strength is lower, but transitions less rapidly than the negative feedback strength can also be used to create an initial ring which could then drive rosette formation. Finally, we note that with the right choice of parameter values, this model can also generate a ring, which could then be used to drive rosette formation (examples of this ring formation can be observed in Fig 5A-F).

Parameter	Description	Value
$k_{disk\ -\ c}$	On disk activation rate of a species modulating c	113 s^{-1}
$k_{basal\ -\ c}$	Off disk/basal activation rate of a species	6.8 s^{-1}

	modulating *c*	
δ_c	Inactivation rate of a species modulating *c*	6.96 s^{-1}
D_c	Diffusion coefficient of a species modulating *c*	0.04 $\mu m^2 s^{-1}$
$k_{disk-\gamma}$	On disk activation rate of a species modulating γ	63.3 s^{-1}
$k_{basal-\gamma}$	Off disk/basal activation rate of a species modulating γ	9.9e-5 s^{-1}
δ_γ	Inactivation rate of a species modulating γ	5.06 s^{-1}
D_γ	Diffusion coefficient of a species modulating γ	4.21 $\mu m^2 s^{-1}$

S1 Note Table A. Parameters for describing diffusing species that modulate the GAP activation rate, *c*, and the self-positive feedback rate, γ.